Organic & Biomolecular Chemistry

Reactivity and Mechanism of α-Nucleophile Scaffolds as Catalytic Organophosphate Scavengers

Journal:	*Organic & Biomolecular Chemistry*
Manuscript ID	OB-ART-02-2019-000503.R1
Article Type:	Paper
Date Submitted by the Author:	19-Mar-2019
Complete List of Authors:	Wong, Pamela; Michigan Nanotechnology Institute for Medicine and Biological Sciences, Internal Medicine Bhattacharjee, Somnath; University of Michigan, Michigan Nanotechnology Institute for Medicine and Biological Sciences Cannon, Jayme; University of Michigan, Michigan Nanotechnology Institute for Medicine and Biological Sciences Tang, Shengzhuang; University of Michigan, Yang, Kelly; University of Michigan, Michigan Nanotechnology Institute for Medicine and Biological Sciences Bowden, Sierra; University of Michigan, Michigan Nanotechnology Institute for Medicine and Biological Sciences Varnau, Victoria; University of Michigan, Michigan Nanotechnology Institute for Medicine and Biological Sciences O'Konek, Jessica; University of Michigan, Michigan Nanotechnology Institute for Medicine and Biological Sciences Choi, Seok Ki; University of Michigan, Michigan Nanotechnology Institute for Medicine and Biological Sciences

Organic & Biomolecular Chemistry

ARTICLE

Reactivity and mechanism of α-nucleophile scaffolds as catalytic organophosphate scavengers

Received 00th January 20xx,
Accepted 00th January 20xx

DOI: 10.1039/x0xx00000x

www.rsc.org/

Pamela T. Wong,[§a,b] Somnath Bhattacharjee,[§a,b] Jayme Cannon,[a,b] Shengzhuang Tang,[a,b] Kelly Yang,[b] Sierra Bowden,[b] Victoria Varnau,[b] Jessica J. O'Konek[a,b] and Seok Ki Choi*[a,b]

Despite their unique benefits imparted by their structure and reactivity, certain α-nucleophile molecules remain underexplored as chemical inactivators for the topical decontamination of reactive organophosphates (OPs). Here, we present a library of thirty α-nucleophile scaffolds, each designed with either a pyridinium aldoxime (PAM) or hydroxamic acid (HA) α-nucleophile core tethered to a polar or charged scaffold for optimized physicochemical properties and reactivity. These library compounds were screened for their abilities to catalyze the hydrolysis of a model OP, paraoxon (POX), in kinetic assays. These screening experiments led to the identification of multiple lead compounds with the ability to inactivate POX two- to four-times more rapidly than Dekon 139—the active ingredient currently used for skin decontamination of OPs. Our mechanistic studies, performed under variable pH and temperature conditions suggested that the differences in the reactivity and activation energy of these compounds are fundamentally attributable to the core nucleophilicity and pK_a. Following their screening and mechanistic studies, select lead compounds were further evaluated and demonstrated greater efficacy than Dekon 139 in the topical decontamination of POX in an *ex vivo* porcine skin model. In addition to OP reactivity, several compounds in the PAM class displayed a dual mode of activity, as they retained the ability to reactivate POX-inhibited acetylcholine esterase (AChE). In summary, this report describes a rationale for the hydrophilic scaffold design of α-nucleophiles, and it offers advanced insights into their chemical reactivity, mechanism, and practical utility as OP decontaminants.

Introduction

Phosphate-based chemical threat agents, collectively referred to as reactive organophosphates (OPs), cause serious life-threatening neurotoxicity upon human exposure.[1, 2] These OPs comprise a broad range of phosphoester compounds ranging from the agricultural pesticides paraoxon (POX), malaoxon and omethoate to the nerve agents sarin and VX, exploited in chemical terrorism (Figure 1).[1, 2] Despite continuing efforts over the past several decades, no single therapeutic agent or regimen has been proven to be fully effective in the treatment of OP intoxication.[1] Increasing threats of OP exposure underscores an urgent need for more effective therapeutic modalities, in particular, by developing OP antidotes with central nervous system (CNS) bioavailability,[3, 4] enzyme-based OP bioscavengers for systemic use,[5-7] and small molecule-based OP scavengers for topical decontamination.[8-10] Here, we present a new approach for the design and validation of small molecule scavengers based on α-nucleophiles. While α-nucleophiles have demonstrated their therapeutic values as OP antidotes over several decades, their potential role as OP scavengers has remained relatively underexplored until recently.[8-11] This article addresses such a significant gap in our current knowledge on the α-nucleophile scavengers by establishing their structure-reactivity trends, determining their molecular and kinetic mechanism of OP inactivation, and evaluating their efficacy in OP decontamination in a skin model.

The biochemical basis of OP neurotoxicity relates to its specific reactivity with acetylcholinesterase (AChE). As the target enzyme, AChE is covalently inhibited by OP through *O*-phosphorylation at serine-203, the catalytic residue in the active site pocket.[12] This enzyme inhibition leads to the rapid accumulation of acetylcholine at the synaptic cleft which results in the symptomatic overstimulation of cholinergic receptors.[1, 13] Current regimens approved for OP intoxication rely on pralidoxime chloride (2-PAM), a primary antidote

[a] Department of Internal Medicine, University of Michigan Medical School, Ann Arbor, Michigan 48109, United States of America.
[b] Michigan Nanotechnology Institute for Medicine and Biological Sciences, University of Michigan Medical School, Ann Arbor, Michigan 48109, United States of America.
§ Equal contributions
* E-mail: skchoi@umich.edu
† Electronic Supplementary Information (ESI) available: [details of any supplementary information available should be included here]. See DOI: 10.1039/x0xx00000x

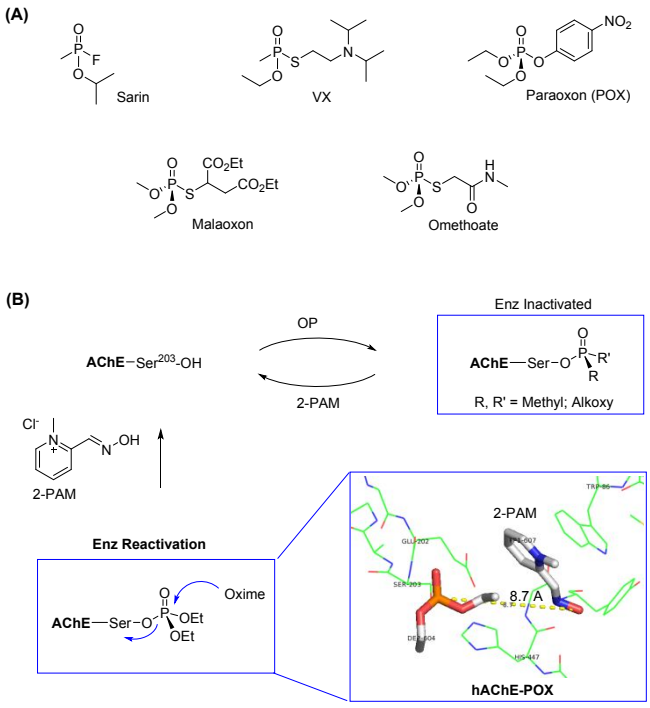

Fig. 1 (A) Representative reactive organophosphates (OPs). (B) Reactivation of OP-inactivated acetylcholine esterase (AChE) by pyridine-2-aldoxime methochloride (2-PAM). Inset: an X-ray crystal structure of POX-inactivated human acetylcholine esterase (hAChE) in complex with 2-PAM (protein data bank (PDB) code 5HFA[12]).

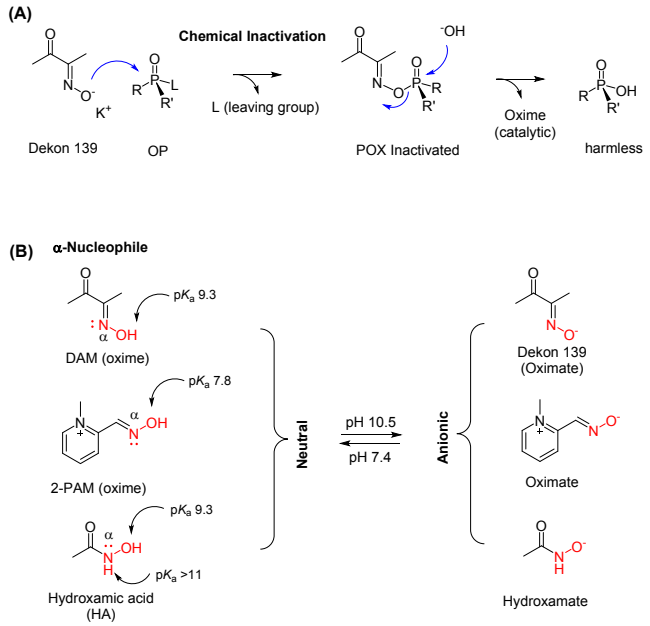

Fig. 2 α-Nucleophilic scavengers of organophosphate (OP). (A) Chemical inactivation of OP by Dekon 139 through a nucleophilic catalytic mechanism. (B) Structures and protonation states of the three α-nucleophiles investigated in this study.

known for its ability to reactivate OP-inhibited AChE (Figure 1), in combination with one or two complementary drugs,[1, 2] which include atropine (a cholinergic receptor antagonist) and an anticonvulsant for epileptic seizure relief. However, despite its essential role in the treatment of OP intoxication, 2-PAM is ineffective for preventing neuronal damage due to its lack of CNS bioavailability,[3, 4] and due to its short half-life (≤ 2 h) in plasma.[14]

In addition to systemic antidote administration, topical decontamination of OPs is essential to effective treatment, as the exposed surface serves as a depot for extended OP absorption, and thus promotes sustained toxicity.[15] Various decontamination kits,[16] materials,[11, 17-20] and methods[21] have been developed that include the FDA-approved reactive skin decontamination lotion (RSDL) for skin decontamination.[22] The active ingredient in RSDL is Dekon 139 (formulated at 1.2 M, pH ≥10.8), a potassium salt of diacetyl monooxime (DAM), which displays strong catalytic reactivity towards OP, leading to its inactivation through hydrolysis (Figure 2). However, despite such beneficial reactivity which is attributable to its α-nucleophilic oxime moiety, Dekon 139 is rapidly absorbed percutaneously as its neutral form, DAM, and can lead to adverse systemic effects such as skeletal muscle paralysis.[23]

Here, we wish to advance our fundamental knowledge in the design and optimization of chemical scavengers for OP inactivation.[8-10, 24] Specifically, we are interested in advancing the chemical strategy for scavenger design based on two well-known α-nucleophile cores, with the goal of improving their reactivity while avoiding the high membrane permeability associated with lipophilic DAM. It involves designing a library of hydrophilic scaffolds of α-nucleophile molecules in which each α-nucleophile core is conjugated to a polar or charged scaffold that acts as a physicochemical modulator.[9] First, we verify the mechanistic aspects of these compounds for their reactivity as OP inactivators.[25, 26] Second, we present their chemical reactivity towards the hydrolysis of POX employed as a model OP measured under pH and temperature-controlled conditions in a high-throughput (HT) colorimetric screening assay, and identify multiple lead compounds based on their rates of POX inactivation. Finally, we evaluate the therapeutic potential of lead compounds for POX decontamination on porcine skin *in vitro*. In summary, we present a rational design strategy that resulted in multiple α-nucleophile scaffolds that display potent reactivity and practical utility as small molecule OP scavengers.

Results and discussion

Design concept of α-nucleophile scaffolds

We designed thirty α-nucleophile compounds of two classes, each containing two functionally orthogonal elements in their structure (Table 1 and 2): (i) a reactive α-nucleophile core and (ii) a covalently linked scaffold (R). The core is the reactive element that engages in the nucleophilic displacement reaction with the phosphoesters for hydrolysis. Of various types of nucleophiles,[26, 27] we selected two α-nucleophiles, pyridinium aldoxime (PAM)[8, 25, 27] and hydroxamic acid (HA),[26, 28, 29] as the reactive cores of our compounds because of their relatively strong reactivity due to the α-heteroatom adjacent to the nucleophilic atom (Figure 2).[26] This current library

includes a few compounds, which were previously reported as enzyme reactivators,[8, 30, 31] however, their potential as OP inactivators remain unknown.

Our design efforts in the PAM core were made with a focus on three subcores with differences in their orientation such that their oxime acidity varies due to electronic effects (pK_a: 2-PAM < 4-PAM < 3-PAM). We also included a set of halogen substituted 4-PAM compounds **8–12**, each with an electronegative Cl or F at the C-3 position. We hypothesized that its high electronegativity in combination with its proximity to the oxime moiety would be able to reduce the pK_a of the oxime. Thus, the pK_a values calculated for these compounds are lowered (7.9–8.0) by approximately 0.3–0.4 units compared to that of the parent 4-PAM (pK_a = 8.3) compound.

Rationale for hydrophilic scaffolds

Absorption of molecules across the skin layer is known to occur primarily through passive diffusion across hydrophobic cellular membranes.[32] As an approach to prevent potential percutaneous absorption associated with small sized or lipophilic α-nucleophile molecules,[33] we conjugated each α-nucleophile core to a scaffold residue (R) consisting of a spacer terminated with a polar or charged handle such as a carboxylic acid, alcohol or primary amine. As compared to the two core types, the structure and functionality of the scaffold domain had more variations as shown in Tables 1 and 2 including in the spacer length (one to three atoms) and composition (carbon, nitrogen and/or oxygen). They were then additionally substituted with a polar group for increased hydrophilicity, such as with a hydroxyl group for the HA class compounds. Spacer groups that were too lengthy, bulky or heavily substituted were not considered because of their unfavourable steric congestion to the reaction center.

Tables 1 and 2 provide summaries of the calculated physicochemical properties of the core-scaffold conjugates. First, each library molecule in the PAM class is larger than DAM (M_r = 101 g mol^{-1}) in size as suggested by their molecular mass (M_r) and calculated molar refractivity (CMR). In addition, each compound has a negative value of *c*log*P* (the partition coefficient between water and 1-octanol[34]) and has more than five H-bond donors/acceptors, supportive of increased hydrophilicity compared to DAM (*c*log*P* = 0.332; four H-bond donors/acceptors).[32, 33] Most compounds in the HA class also show such improved properties that are considered to help reduce the permeability of a molecule across the skin layer.[33] Second, the core acidity for both classes as predicted by the

Table 1 Library of pyridinium aldoxime (PAM) scaffold compounds

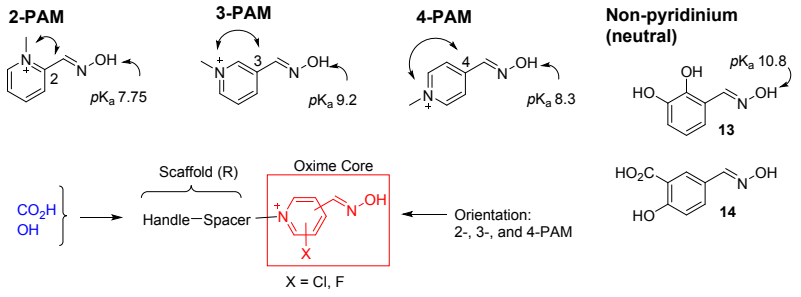

Compound Number	Structure		pK_a (oxime)[a,b]	*c*log*P*[a]	CMR[a]
	Oxime Core (X)	Scaffold (R)			
Dekon 139	DAM	-	9.32	0.332 (−0.114)[b]	2.717
2-PAM	2-PAM	H_3C-	7.75	−3.666	4.142
1	2-PAM	HO_2CCH_2-	8.0	−6.783	4.795
2	3-PAM	HO_2CCH_2-	9.2	−6.783	4.795
3	3-PAM	$HO_2C(CH_2)_2$-	9.2	−6.287	5.259
4	3-PAM	$HO(CH_2)_2$-	9.2	−3.509	4.759
5	4-PAM	HO_2CCH_2-	8.3	−6.783	4.795
6	4-PAM	$HO_2C(CH_2)_2$-	8.3	−6.287	5.259
7	4-PAM	$HO(CH_2)_2$-	8.3	−3.509	4.759
8	4-PAM (3-Cl)	HO_2CCH_2-	7.9	−6.721	5.286
9	4-PAM (3-Cl)	$HO_2C(CH_2)_2$-	7.9	−6.226	5.75
10	4-PAM (3-Cl)	$HO(CH_2)_2$-	7.9	−3.447	5.251
11	4-PAM (3-F)	HO_2CCH_2-	8.0	−7.041	4.810
12	4-PAM (3-F)	$HO_2C(CH_2)_2$-	8.0	−6.546	5.274
13	Non-pyridinium	HO-	10.8	1.830	4.107
14	Non-pyridinium	HO_2C-	10.6	−3.159	4.607

Abbreviations: pK_a = −log(K_a). *P* = partition coefficient between water and 1-octanol; calculated *c*log*P* = log([oxime]$_{1\text{-octanol}}$/[oxime]$_{water}$). CMR = calculated molar refractivity (m^3 mol^{-1}). Physicochemical parameters calculated by ChemDraw Software (Professional 16.0)[a] or Advanced Chemistry Development (ACD/Labs) Software V11.02 (©1994-2017).[b]

Table 2 Library of hydroxamic acid (HA) scaffold compounds Library of pyridinium aldoxime (PAM) scaffold compounds

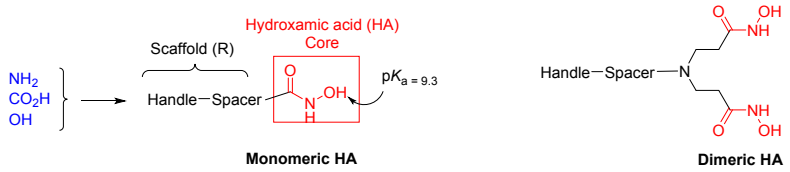

Compound Number	Structure: Scaffold (R)	pK_a (HA)[a,b]	clog*P*[a]	CMR[a]
15	HO_2CCH_2-	8.4	−1.524 (−0.811)[b]	2.315
16	$HO_2C(CH_2)_2$-	9.1	−1.562 (−0.711)[b]	2.779
17	$HO_2C(CH_2)_3$-	9.3	−1.245 (−0.436)[a]	3.243
18	$HO_2CCH_2NHCH_2$-	6.8	−3.871	3.148
19	$HO_2CCH_2N(CH_3)CH_2$-	6.8	−3.115	3.611
20	$HO_2CCH_2OCH_2$-	8.9	−1.562	2.932
21	$HO_2CCH_2C(CH_3)_2CH_2$-	9.3	−0.447	4.170
22	$HOCH_2$-	9.5	−1.855	1.816
23	$H_2N(CH_2)_2$-	8.6	−1.909	2.495
24	$HN(CH_3)CH_2$-	10.1	−1.857	2.495
25	$HO(CH_2)_3$-	9.3	−1.701	2.743
26	$H_2NCH(CH_2OH)$-	9.0	−2.928	2.648
27	$H_2NCH(CH_2CO_2H)$-	9.0	−3.542	3.516
28	Dimer HO_2CCH_2-	8.8	−3.580	5.560
29	Dimer $HO(CH_2)_2$-	8.8	−2.12	5.525
30	Dimer $HO_2C(CH_2)_2$-	8.8	−4.305	6.024

For abbreviations, see Table 1. Physicochemical parameters calculated by ChemDraw Software (Professional 16.0)[a] or Advanced Chemistry Development (ACD/Labs) Software V11.02 (©1994-2017)[b]

pK_a value shows variations depending on the core type, substitution group and scaffold moiety. In general, the PAM core family of compounds have a lower range of pK_a's (7.9–9.2) than the HA core family compounds (8.4–9.3). However, most compounds in the library showed lower pK_a values than DAM (9.32) with the exception of only a few compounds in the HA class.

Synthesis of α-nucleophile scaffolds

As methods for PAM compound synthesis, we used the quaternary *N*-alkylation of pyridine aldoxime, the approach well established for preparing enzyme reactivators.[8, 30, 31] Compounds **1–7** in the PAM series were prepared by the *N*-alkylation of pyridine-n-aldoxime (n = 2, 3, or 4) with a requisite halogen (Br, I)-terminated alkane scaffold such as iodoacetic acid, 2-bromoethanol and 3-bromopropionic acid as detailed in the Supporting Information (SI). PAM compounds **8–12**, each with a chlorine or fluorine substitution at the C-3 position, were prepared similarly except for the use of 3-chloro or 3-fluoropyridine aldoxime. Two non-pyridinium oxime compounds **13**, **14**, which show lower oxime acidity than the PAM compounds, were prepared as controls from their corresponding aldehydes by treatment with hydroxylamine.

The synthesis of scaffold compounds **15–30** in the HA class was performed conveniently in a one-step process through the hydroxyamidation reaction of an anhydride or ester molecule with hydroxylamine in methanol (details in the SI). Their reactants were selected from cyclic anhydrides (e.g., glutaric, succinic), α/β-amino acid esters (*N*-methyl glycine, β-alanine, L-serine methyl ester) and linear monoesters terminated with a carboxylic acid or hydroxyl group at the other end. Dimeric scaffold compounds **28–30** were prepared by applying the same method from the corresponding dimeric esters.

Each compound in both classes was fully characterized for its identity and homogeneity (≥95%) using standard analytical methods that included ^{1}H and ^{13}C NMR spectroscopy, mass spectrometry, and ultra-performance liquid chromatography (UPLC) as detailed in the SI. Compound stability was tested for selected compounds in phosphate buffered saline (PBS) at pH 10.5, the condition that is used in the formulation of Dekon 139 in RSDL (Figure S2). UPLC analysis indicated no evidence of compound degradation at pH 10.5 after incubation for at least three days at ambient temperature.

Nucleophilic catalysis of POX hydrolysis

Figure 3 shows proposed mechanisms of OP inactivation applied for POX with Dekon 139.[9, 25, 26, 35] The OP inactivation

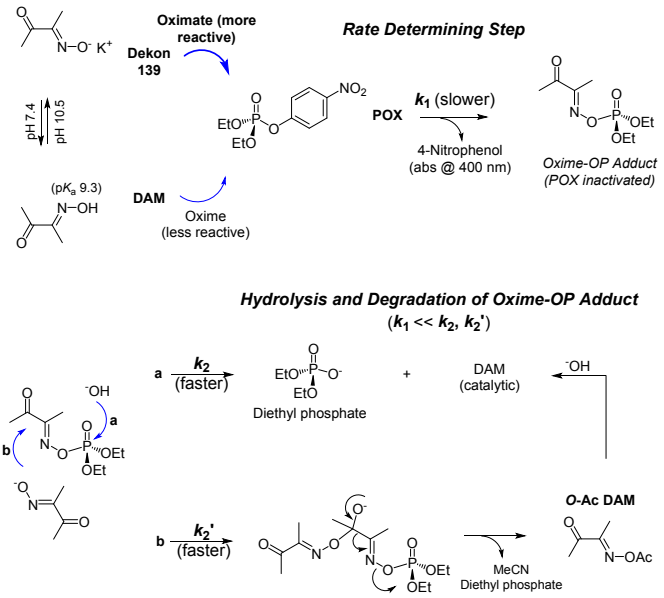

Fig. 3 Kinetics and mechanism of paraoxon (POX) inactivation by Dekon 139. The rate is determined by the nucleophilic attack at the first step (rate constant k_1) which occurs much more slowly than the subsequent hydrolysis of an oxime-POX adduct (k_2)[9] and/or the potential degradation via Beckmann fragmentation (k_2').[35]

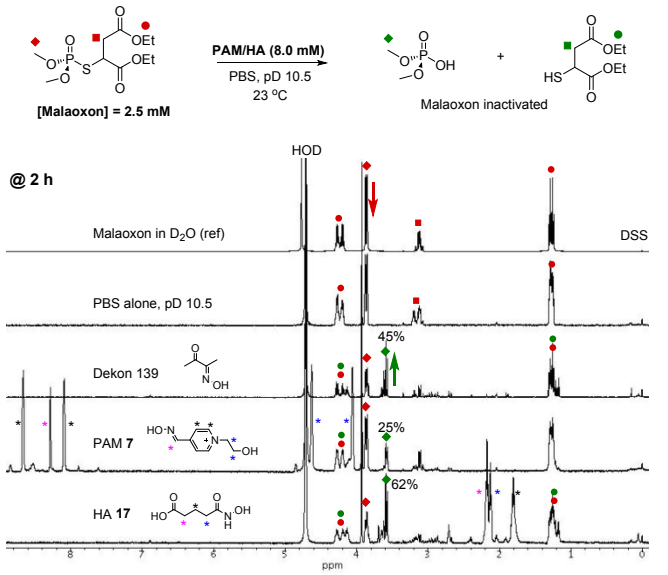

Fig. 4 ^{1}H NMR spectral traces of the hydrolysis of malaoxon (2.5 mM) in a deuterated phosphate buffered saline (dPBS, pD 10.5) alone, or catalysed by Dekon 139 (8.0 mM), **7** (8.0 mM), and **17** (8.0 mM), each in pD 10.5 at 23 °C after 2 h. The fraction (%) of malaoxon hydrolysed was estimated by the integration of its signals for OMe groups.

occurs in two steps: (i) a slower nucleophilic attack that results in an OP-oxime (DAM) adduct; (ii) the faster degradation of the adduct. Thus, the overall rate of OP inactivation shows dependency on rate constant (k_1) in the first step. Compared to the first step that involves a single mechanism, the second step could involve two mechanisms as shown in Figure 3 (lower). These include catalytic hydrolysis[9] or stoichiometric degradation via Beckmann fragmentation,[24, 35] each contributing to a variable extent under certain reaction conditions.

To verify the applicability of such mechanisms to the current library compounds, we performed ^{1}H NMR experiments for two representative compounds, **7** and **17,** by reacting POX (2.5 mM) with either compound added at 8.0 mM in deuterated phosphate buffered saline (dPBS, pD 10.5). Overlaid ^{1}H NMR spectra showed the time-dependent decrease of POX signals as reflected by the appearance and increase of new peaks corresponding to 4-nitrophenol (4-NP) and diethyl phosphate (Figure S3). No POX was detectable after 24 h of inactivation by compounds **7** and **17**, indicating complete POX inactivation with half-life ($t_{1/2}$) than Dekon 139, which still had ~50% intact POX remaining after the same period. As a control, POX alone (pH 10.5) remained fully stable over 72 h.

The NMR spectral traces of these compounds show evidence for catalytic POX hydrolysis because signals corresponding to **7** or **17** remained largely unchanged in each spectral set. Certain degradation products such as MeCN or *O*-Ac DAM were not detectable that might result from a second-order Beckmann fragmentation as suggested earlier for Dekon 139[24, 35] under non-aqueous conditions (path b; Figure 3). This lack of spectral changes is supportive of a catalytic function for compounds **7** and **17** in POX hydrolysis (path a) rather than stoichiometric consumption (path b).

In addition to POX, we performed similar ^{1}H NMR experiments using two other OP surrogates, malaoxon and omethoate, each having a P-S bond like VX. As shown in the overlaid spectra (Figure 4, Figure S3E), compounds **7** and **17** showed evidence for their catalytic reactivity. For example, malaoxon remained intact in PBS (pD 10.5) for 2 h (up to 24 h; not shown). However, it was inactivated rapidly by **7** or **17**, each displaying $t_{1/2}$ (calculated from decay curves) of 2.7 h and 0.6 h, respectively, which is comparable to or better than Dekon 139 (2.9 h).

In summary, ^{1}H NMR experiments performed with three OP surrogates (POX, malaoxon, and omethoate) provide new evidence for the mechanism of OP inactivation by **7** and **17** as nucleophilic catalysts. This result strongly supports their broad reactivity for catalytic cleavage of both P-O and P-S bonds.

Reaction kinetics by colorimetric assay

Performing a colorimetric assay enables to measure the kinetics of POX inactivation due to the release of 4-NP (absorbance at 400 nm) upon its hydrolysis, as illustrated in the UV–Vis spectral traces (Figure S4). It also has amenability to a microplate reader, which offers high-throughput (HT) capabilities for compound screening.[8, 9]

Following this HT method, we monitored POX hydrolysis at 37 °C by adding a fixed concentration of POX (30 μM) to a test compound formulated at four different concentrations (0.5–8.0 mM). The large molar excess of the test compound allows the determination of the rate constant k_1 under pseudo first-order conditions. Compound screening was performed at pH 7.4 and 10.5 in order to compare the reactivity of each test compound in the neutral oxime or hydroxamic acid form (≥95%, pH 7.4) or in the negatively charged oximate or

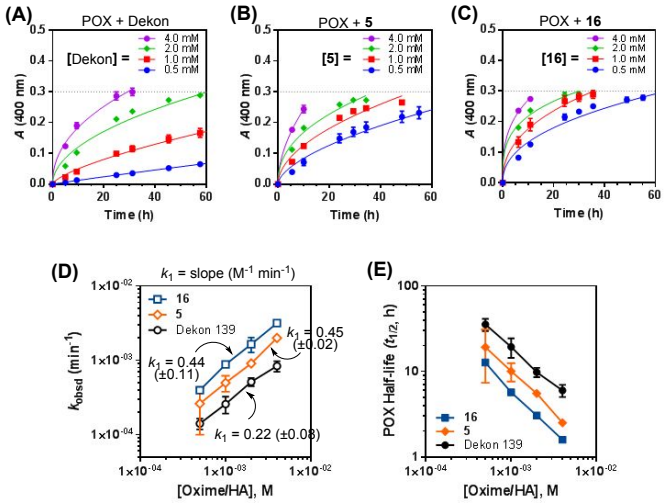

Fig. 5 (A–C) Kinetic traces of paraoxon (POX, 30 μM) hydrolysis catalysed by Dekon 139, **5** and **16** in PBS, pH 10.5 at 37 ˚C. (D, E) k_{obsd} and POX half-life $t_{1/2}$ (= log(2)/k_{obsd}) plotted as a function of compound concentration. k_1 refers to a bimolecular rate constant obtained from linear regression analysis. Data points are mean ± standard deviation (SD) (n ≥ 3).

hydroxamate form (≥95%, pH 10.5) as predicted by the Henderson-Hasselbalch equation.[36]

Figure 5 shows reaction kinetics of POX hydrolysis performed at pH 10.5 as illustrated with Dekon 139 and two representative compounds, **5** and **16**. Growth curves in Figure 5A–5C suggest 4-NP production as a function of time and compound concentrations. Regression analysis of each curve provided an observed rate constant k_{obsd} (min^{-1}) as the slope of absorbance (A) growth ($\Delta A/\Delta t$) at each concentration, and calculated the POX half-life ($t_{1/2}$ = log(2)/k_{obsd}). The plots of k_{obsd} and $t_{1/2}$ values presented in Figures 5D and 5E show that Dekon 139 is less effective for POX inactivation than **5** and **16** given its lower k_{obsd} values and accordingly, longer half-life values. As defined in Figure 3, a bimolecular rate constant k_1 was obtained from k_{obsd}-concentration plots under pseudo-first order conditions.[8, 25] Comparison of individual k_1 (M^{-1} min^{-1}) values indicates approximately 2-fold lower reactivity of Dekon 139 (0.22) compared to **5** (0.45) and **16** (0.44) which display almost equal reactivity.

In summary, the colorimetric assay illustrated with these representative library compounds shows that the rate of POX inactivation is dependent on both compound reactivity and the test concentration of the compound, which is inversely correlated with POX half-life. Each linear regression plot for a test compound (Figure 5E) serves as an important tool for us to predict an optimal scavenger concentration for faster POX inactivation, such as 0.3 M to reach a target half-life of ≤10 min, as applied in the topical decontamination of POX as described later.

Screening of library compounds

Under the same microplate condition, we performed screening of all compounds **1**–**30** for their reactivity of POX hydrolysis. The rate constants (k_{obsd}, k_1) summarized in Figure 6 show significant variations dependent on α-nucleophile types and

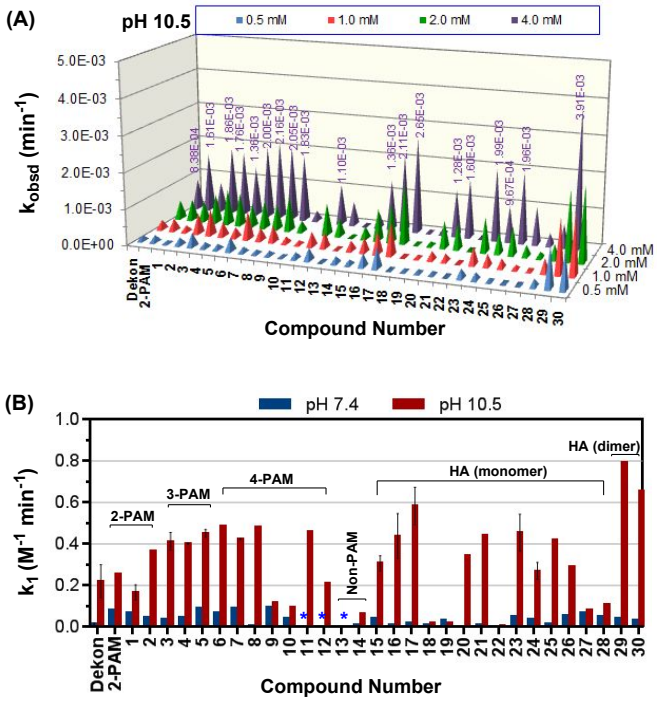

Fig. 6 Rate constants for POX hydrolysis catalysed by library compounds **1**–**30**. (A) k_{obsd} (min^{-1}) measured for 30 μM POX with various concentrations of test compounds (0.5–4.0 mM, pH 10.5) at 37 (±1) ˚C. k_{obsd} values at 4.0 mM of the test compound are indicated in purple. (B) Plots of k_1 (M^{-1} min^{-1}) at pH 10.5 and 7.4. * Not determined due to compound instability or lack of activity.

pH conditions. This primary screening led to the identification of 14 lead compounds in both classes which include **2**–**8** (PAM), and **16**, **17**, **21**, **23**, **25**, **29**, **30** (HA). Each of these shows reactivity (k_1) ~2 to 4 times greater than Dekon 139 at pH 10.5.

Use of Cl or F-substituted 4-PAM resulted in reactivity not as effective as would have been anticipated based upon their lowered pK$_a$. Except **8**, these compounds **10**–**12** displayed undesirable reaction properties such as non-catalytic consumption and/or partial degradation even at pH 7.4 as evident by ^{1}H NMR and mass spectrometry analyses (not shown). As controls, two non-pyridinium compounds, **13** and **14**, showed either a non-detectable or a very low level of reactivity, emphasizing the essential role played by the core.

The results also show pH-dependent variations in reactivity.[8, 9] At pH 10.5, POX hydrolysis was faster by up to an order of magnitude as compared to at pH 7.4. This result confirms our general postulation that the greater reactivity relates to the oximate or hydroxamate anions, which are the predominant species (>95%) at pH 10.5 (Figure 2), compared to the neutral species which predominates at pH 7.4.

Structure-reactivity correlation

We observed certain structure-reactivity trends in the core and scaffold domain. First, core type appears to account for generic differences in reactivity observed between the two α-nucleophile classes. At pH 7.4, rate constants are broadly higher by PAM compounds (Figure 6B), which display lower pK_a values (pK$_a$ = 7.75–9.2; Table 1) and thus higher fractions (Fr) of the oximate anion. Such core-dependent differences

disappear at pH 10.5 in which each oxime or HA core is deprotonatable predominantly to its anionic species ([Oximate/Hydroxamate]/[Oxime/HA] = $e^{[pH - pKa]}$).[36]

In the PAM class, the core orientation plays a fundamental role in determining reactivity. Greater reactivity is with the compounds **6**–**8** in the 4-PAM subclass than in the 3-PAM or 2-PAM subclass. Our result is in line with an earlier report which predicts higher Brønsted-type nucleophilicity for 4-PAM relative to 2-PAM.[27] In addition to this core nucleophilicity and its associated acidity (pK$_a$), we attribute such greater reactivity to the lower steric congestion of the 4-PAM core in its nucleophilic attack on the phosphoester center.

Lastly, the scaffold structure most frequently found in lead compounds from the PAM class is composed of a two-carbon spacer terminated with a hydroxyl or carboxylic acid group. However, it appears to have less of an impact on reactivity than the orientation of the PAM core. Similarly, good scaffolds that were found in the HA class are composed of a two or three-carbon spacer. In contrast, scaffolds which are based on a single carbon spacer were less reactive than those with longer carbon spacers such as **15** (1 CH_2) compared to **16** (2 CH_2) and **17** (3 CH_2). It is also notable that scaffolds with a single carbon spacer terminated with an amine or hydroxyl group such as **18**, **19**, **22**, and **27** were much less reactive than those with longer carbon spacers, pointing to unfavourable electronic and steric effects.

Role of physicochemical parameters

In our library design, we varied three physicochemical properties for two independent purposes: i) core acidity (pK$_a$) as a primary determinant for enhancing OP reactivity; ii) scaffold hydrophilicity and size, each as a physicochemical modulator for addressing percutaneous penetration.[33] We determined the extent of the correlation of these properties with reactivity as presented in Figure 7A, 7B (core acidity) and Figure S5 (hydrophilicity, size).

First, higher core acidity led to greater reactivity for the majority of compounds (upper left quadrant). The correlation analysis of these plots suggests a positive (inverse) correlation between core acidity (pK$_a$) and reactivity despite relatively low values for the coefficient (r). Thus, these analyses suggest the significant role of core acidity in dictating reactivity. Second, plotting of reactivity versus physicochemical modulators, *c*Log*P* (a predictor for hydrophilicity) and CMR (size), showed a weak but positive correlation (Figure S5). It suggests that the optimization of physicochemical properties does not make a negative impact on the reactivity of the library compounds.

pH Models of POX hydrolysis

As briefly discussed in the library screening above, the pH of the reaction media plays a critical role in the rate of POX hydrolysis because the fraction of reactive oximate or hydroxamate species varies with pH. To quantitatively formulate the pH dependence of the rate, we performed reaction kinetics at variable pH conditions for Dekon 139 and selected lead compounds in the PAM (**1**, **3**–**5**, **7**) and HA (**15**–**17**, **23**, **24**) class, as presented in the plots of Figures 7C–7F and

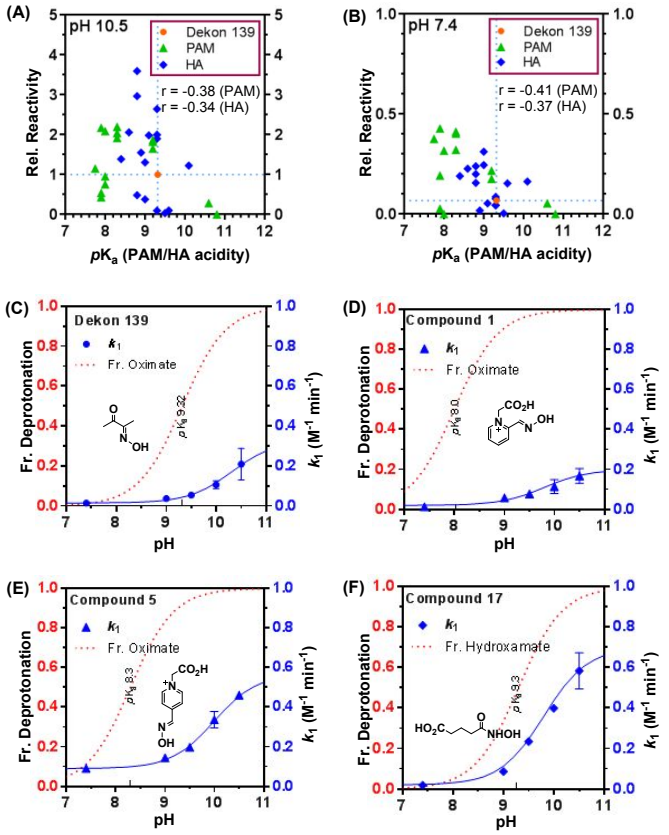

Fig. 7 Effect of pK$_a$ and pH on reactivity. (A, B) Plots of reactivity versus core acidity (pK$_a$) at pH 10.5 and pH 7.4. (C–F) Plots of k_1 (37 °C) and the fraction (Fr) of deprotonation[36] as a function of medium pH for representative compounds. Relative reactivity refers to the ratio of k_1(test compound)/k_1(Dekon 139, pH 10.5). r = correlation coefficient (Pearson)

Figure S6. Each plot shows the rate of POX hydrolysis (k_1) as a function of medium pH (7.4–10.5) along with the predicted fraction of oximate or hydroxamate species present (deprotonation fraction = $e^{[pH - pKa]}$[36]). Each plots also shows a fitting curve (blue line) generated to model the reactivity-pH relationship based on a linear combination of two parallel catalytic pathways for POX hydrolysis—one through a neutral species, and the other through an anionic species (Figure 3).

Each compound shows maximal reactivity at pH 10.5 as anticipated by the greater fraction of oximate or hydroxamate species (fraction ≥ 0.95; red dotted line). The reactivity decreases as the fraction of anionic species decreases at the lower pH. These pH models also show that core pK$_a$ does not solely account for the pH-dependent variation in reactivity among lead compounds. This is evident by the two orientation isomers **1** (Figure 7D) and **5** (Figure 7E) in the PAM class. Despite having identical scaffolds, compound **1** (pK$_a$ = 8.0) shows lower reactivity than **5** (pK$_a$ = 8.3) over the entire range of pH conditions. Thus, these pH models provide evidence that corroborates the effect of the oxime orientation or perhaps steric congestion as discussed above. In summary, we built pH models of POX hydrolysis for the lead compounds that correlate compound reactivity with the fraction of core deprotonation.

Temperature effect

In addition to compound screening at 37 °C, we evaluated reaction kinetics at two lower temperatures, 2 °C and 17 °C, to gain insights into the thermodynamics of POX hydrolysis. Figure 8 summarizes the results acquired with the selected compounds, showing that k_1 is temperature dependent at both pH conditions. At pH 10.5, Dekon 139 showed an increase in k_1 by a factor of 2.9 or 2.0 as the temperature was raised from 2 °C to 17 °C or 17 °C to 37 °C, respectively. This temperature effect occurred similarly across all of the tested compounds.

Activation energy (E_a) associated with POX hydrolysis was calculated according to the Arrhenius equation, $\ln(k_1) = \ln(A) - (E_a/R)(1/T)$ where A, R and T refers to a pre-exponential factor, gas constant and absolute temperature (K), respectively. As summarized in Figure 8C, E_a values are positive, indicating endothermic process of POX hydrolysis by PAM and HA compounds. Their values are generally lower at pH 10.5 than at pH 7.4. These differences are attributable to the higher reactivity of the deprotonated core species.

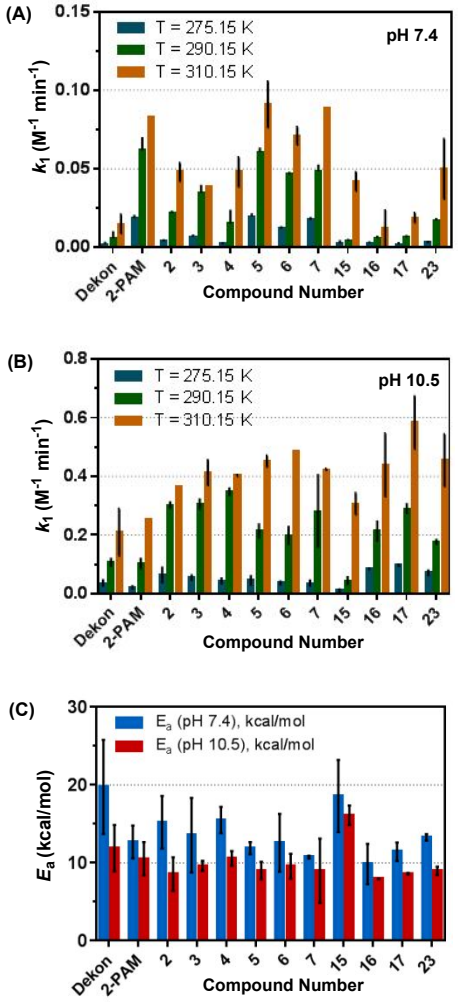

Fig. 8 Effect of temperature on POX hydrolysis kinetics. (A, B) k_1 plotted as a function of temperature at pH 7.4 and pH 10.5. (C) Activation energy (E_a). Each k_1 value represents a mean ± SD (n ≥ 3) at a given temperature (±1 °C).

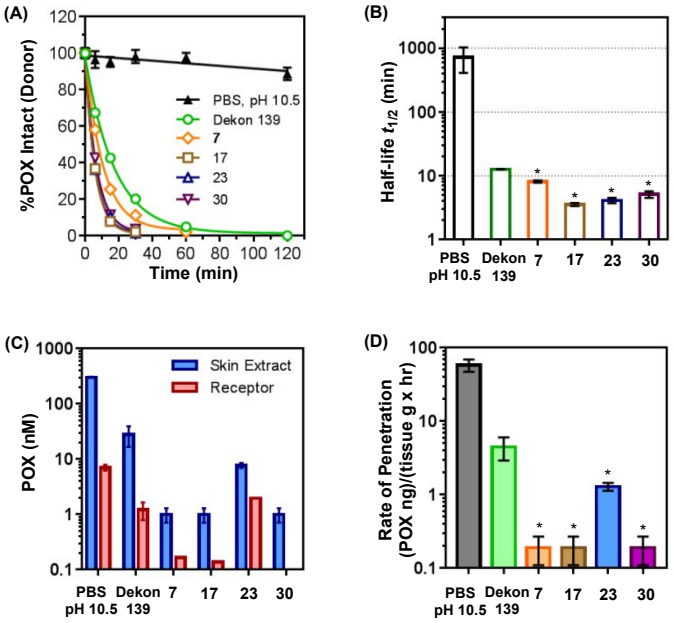

Fig. 9 POX decontamination on porcine skin *ex vivo* by treatment with selected lead compounds in a Franz cell. Fraction of intact POX remaining (% area under curve) (A) and POX half-life in the donor compartment (B). Amount (nM) of POX detected in the skin extract and receptor compartment (C), and the rate of skin penetration of POX after treatment (D). Each value represents a mean ± SD (n = 2–4). *p < 0.05, one-way ANOVA for each compound compared to Dekon 139.

Skin decontamination of POX *ex vivo*

For validating the practical use of the α-nucleophile library compounds, we selected four lead compounds, **7**, **17**, **23**, and **30**, based on their core class, scaffold diversity and reactivity (Figure 6). We investigated their effectiveness in POX decontamination in a skin model in a Franz cell (Figure 9). Use of POX as an OP surrogate for skin penetration offers benefits because of its similar lipophilicity (clog$P$ = 1.98) close to prominent OP molecules such as VX (clog$P$ = 2.28). As described in our previous report, a patch of porcine skin (dehaired, thickness = 1.5 mm) was clamped between the donor and receptor chambers (Figure S7).[9] The skin surface was pre-exposed to POX (50 μM), and immediately after 2 min, was treated for 2 h with Dekon 139 or each compound at 0.3 M, or with a vehicle control (PBS, pH 10.5).

The kinetics of POX hydrolysis in the donor chamber was determined by UPLC analysis of the remaining POX in the donor chamber over the treatment time (Figure 9A, 9B). As anticipated, treatment with Dekon 139 and each test compound showed a rapid decay curve for POX as compared to the PBS treatment (pH 10.5) in which POX remained largely stable. The effectiveness of the test compounds was evident with POX half-life ($t_{1/2}$ = 12.7 min) values calculated from individual decay curves: **7** (8.2 min); **17** (3.6 min); **23** (4.1 min); **30** (5.1 min). All of the compounds were more effective than Dekon 139 ($t_{1/2}$ = 12.7 min) and the PBS vehicle control (720 ± 311 min) (p < 0.05).

We quantified the fraction of POX that undergoes skin penetration, and subsequently flows through to the receptor chamber by LC MS/MS spectrometry (limit of quantitation or

LOQ ≈ 1 nM). Figure 9C shows that the skin treated with the PBS vehicle contained the highest amount of POX (304 ± 7 nM) as compared to the skin treated with Dekon 139 (28.1 ± 11.4 nM), **7** (≤1.0 ± 0.3 nM), **17** (≤1.0 ± 0.3 nM), **23** (7.7 ± 0.8 nM) or **30** (≤1.0 ± 0.3 nM). The concentration of POX (nM) in the skin extract was converted to the rate of skin penetration (= POX (ng)/[skin weight (g) × h]) as a normalized unit indicative of decontamination efficacy. As shown in Figure 9D, each lead compound showed a decrease in the penetration rate larger than Dekon 139 (4.9 ± 1.6) or the PBS control (58.4 ± 11.1; *p* value < 0.05).

In the receptor chamber, the amount of POX detected was much lower than that in the skin for each treatment. Such preferred distribution in the skin could be attributable to the high lipophilicity of POX.[34] In summary, this result demonstrates the improved efficacy of the four lead compounds as compared to Dekon 139 in skin decontamination of POX *ex vivo*.

Reactivation of POX-inhibited AChE

In the experimental designs above, we focused on screening and identifying lead α-nucleophile scaffolds as potent OP scavengers. These results provide clear evidence supportive of their potent utility for topical OP decontamination. In addition to this main objective, we were also interested in certain α-nucleophiles for their inherent ability that pertains to the reactivation of OP-inactivated AChE.

Of the two nucleophilic cores employed here, the PAM core has the potential ability to reactivate OP-inhibited AChE as well established with 2-PAM and obidoxime.[37-39] Here, we investigated whether hydrophilic PAM compounds retain such activity using AChE (*Electrophorus electricus*; 0.1 U/mL) in PBS, pH 8.0 at 23 °C according to Ellman's method.[40, 41] As shown in Figure 10A, POX showed dose-dependent inhibition of AChE activity with IC_{50} of 50 nM (calculated) as reported in the literature.[42] 2-PAM and obidoxime were then tested for their ability to reactivate AChE pre-inhibited by treatment with POX (500 nM) for 60 min. As anticipated, they showed activity for AChE reactivation in a dose-dependent manner to a maximal level of 67% by 2-PAM (0.1 mM) and 70% by obidoxime (0.01 mM) (Figure 10B).

A dozen of library compounds were similarly tested in this enzyme assay, and only three compounds **5**–**7**, all in the 4-PAM subclass, were found to show AChE reactivation activity to a various degree (Figure 10B). Observation of their activity is notable, as other PAM compounds including **3** in the 3-PAM subclass and **29** and **30** in the HA class failed to show any activity at the same dose range (not shown). Among the three compounds, **7** was most active, and though less active than 2-PAM or obidoxime, it continued to increase its reactivation activity up to 37% at 1.0 mM. Like 2-PAM and obidoxime, **7** showed enzyme inhibition in a dose-dependent manner (Figure 10C), which could be attributable to their intrinsic ability to inhibit the enzyme via competitive occupation in the catalytic pocket.[43, 44] Differences in the reactivation activity among the three 4-PAM compounds are attributable to the structural difference in their scaffold. Conjugation with a

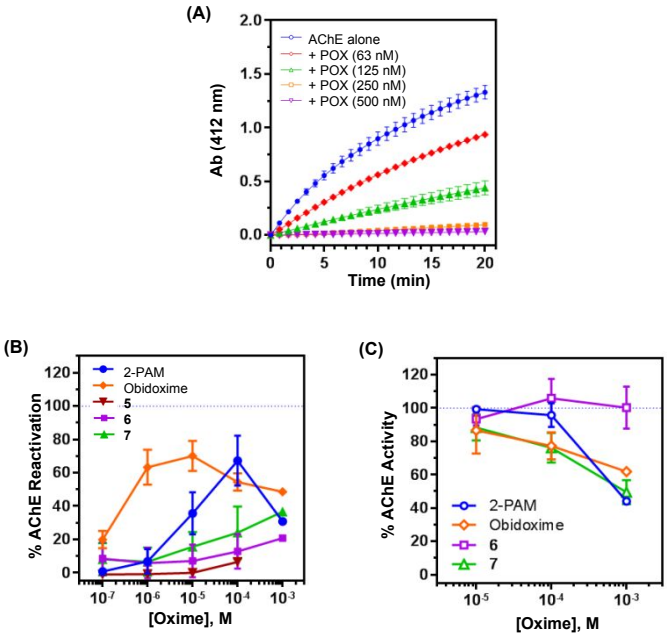

Fig. 10 Reactivation of POX-inhibited AChE (*Electrophorus electricus*) by oximes **5**–**7**. (A) Kinetic traces of enzyme activity showing dose-dependent inhibition by POX. (B) Compound efficiency in the reactivation of AChE pre-inhibited by POX (500 nM). (C) Effects of oximes alone on AChE activity.

neutral hydroxyl scaffold (**7**) is more effective for reactivation activity than a negatively charged scaffold (**6**). In summary, compounds in the 4-PAM subclass retain the ability to reactivate AChE inhibited by POX. This activity may serve as an additional benefit in their use for skin decontamination. Having such activity is not necessary for OP decontamination, but its determination would be valuable for expanding our knowledge base in the design of enzyme reactivators, and potentially as an early lead in the design of multifunctional antidotes for treating OP exposure.[45]

Conclusion

This study offers significant advances in the design of α-nucleophile compounds as the chemical scavengers of OPs. Despite its essential role in skin decontamination, Dekon 139 suffers from adverse systemic effects arising from the rapid percutaneous absorption of its neutral form, DAM.[23] In this work, we investigated a core-scaffold binary approach in the design of potent small molecule scavengers of OPs in which the scaffold involves to improve a physicochemical property while each linked α-nucleophile core directly engages in the catalytic reaction. We prepared and tested 30 library compounds, which show improvements in their molecular size, hydrophilicity, and/or core acidity than DAM. We presented NMR evidence supportive of their catalytic reactivity against three OP surrogates (POX, malaoxon, omethoate), each having a P-O or P-S bond. We identified 14 reactive compounds highly effective for catalysing POX hydrolysis using a colorimetric assay under variable pH and temperature conditions. Some of

these further displayed greater efficacy for POX decontamination in a skin model as compared to Dekon 139.

Oure results offer significant insights into the practice of OP decontamination. Our pH models established with multiple lead compounds suggest that compound formulation should be performed at or above the pH that leads to the significant fraction of core deprotonation (≥95%) for high reactivity. Variable temperature models, which verified the endothermic pathway associated with POX hydrolysis catalysed by α-nucleophile compounds, provide solid evidence for applying decontaminant solutions at temperatures as high as permitted by the skin.

Finally, the chemical handle terminating each scaffold allows further modifications of the lead compound into a much larger construct through its covalent attachment to a polymer molecule or nanoscale carrier. As reported in the design of delivery systems for antidote drugs[8, 46-48] and bioscavengers,[17] such oxime/HA-polymer conjugates can be highly advantageous in topical applications as they provide an excellent route to further reduce percutaneous permeation and facilitate extended duration of action via polymer pharmacokinetics.[49] This aspect of nanoscale scavenger design will constitute the subject of future studies.

Overall, we identified multiple lead compounds from the current library of α-nucleophile scaffolds that offer substantial benefits as OP scavengers based on their structure-reactivity trends, their catalytic mechanism of OP inactivation, and their potent efficacy demonstrated for POX decontamination in the skin model. These results strongly support their development potential as the topical decontaminant of OPs.

Experimental section

Synthesis of α-nucleophile scaffolds

Full details for compound synthesis and characterization (**1–30**) are provided in SI with references cited therein. Copies of spectral data are also provided for the selected compounds including ^{1}H NMR spectra, mass spectra and UPLC traces.

^{1}H NMR spectroscopy

The NMR experiments for POX hydrolysis were performed at room temperature (23 ± 1 °C).[8, 9, 48] In a typical experiment, Dekon 139 or a test compound, each prepared at 8.0 mM in a deuterated PBS buffer (pD 10.5), was mixed with POX at 2.5 mM. The kinetics was monitored under a standard acquisition condition[46, 47] by collecting spectra at variable time points as specified in Fig. S3.

UV–Vis spectrometry

The kinetics of POX hydrolysis by UV–Vis spectrometry was performed as reported earlier.[8, 9] POX (30 μM) was added to a test solution prepared at 4.0 mM in PBS, pH 10.5 at 37 °C. The fraction of POX hydrolysed was determined by measuring an increase in 4-NP absorbance at 400 nm (Figure S4).

Colorimetric screening of compound reactivity

As a primary method for compound screening of POX hydrolysis, a colorimetry assay was performed in a plate reader (Synergy™, BioTek). In a representative experiment, Dekon 139 or a test compound formulated in PBS at either pH 10.5 or 7.4 was loaded in a 96-well microplate (180 μL; n = 3) and serially diluted 2-fold using the same buffer to a range of test concentrations (0.5–8.0 mM). A POX solution (20 μL, 0.30 mM) freshly prepared in the test PBS condition was then added to each test well. Immediately after mixing, the microplate was read in an absorbance mode (400 nm). After this first read ($A_{t=1}$), the plate was incubated in a temperature-controlled environment such as at 37 (± 1) °C, and it was taken out shortly for reading at variable time points ($A_{t=2}$ to $A_{t=8}$) as specified in Figure 5.

Rate constants of POX hydrolysis

Data analysis for determining rate constants was performed as previously reported.[8] First, absorbance at a specific time point ($\Delta A_{t=n}$) was calculated by subtraction of the first read ($A_{t=n} - A_{t=1}$). Second, standard calibration curves of 4-NP absorbance vs. concentration were acquired in the range of 0.1–100 μM in PBS at two different pH conditions: A (400 nm) = slope × [4-NP]; slope = 1.01 (±0.02) × 10^{-4} at pH 10.5, and 1.46 (±0.03) × 10^{-4} at pH 7.4. Each curve was used to calculate the concentration of 4-NP produced ($[4\text{-NP}]_{t=n}$) and thus POX remaining ($[POX]_{t=n} = 3.0 \times 10^{-5}$ M − $[4\text{-NP}]_{t=n}$). Rate constants for POX hydrolysis were extracted according to a second-order rate law under pseudo-first order conditions ([PAM/HA] >> [POX]; Eq 1–Eq 4). The bimolecular rate constant k_1 was determined as the slope of the linear plot of k_{obsd} versus PAM/HA concentration (Eq 2). The values of the kinetic parameters including k_{obsd} and POX half-life ($t_{1/2}$) are reported as a mean (±SD) value obtained from at least three independent measurements (n ≥ 3).

$$\text{Rate} = -d[POX]/dt \approx k_1[POX][PAM/HA] \text{ where } k_1 << k_2 \quad \text{Eq 1}$$

$$\text{Rate} = k_{obsd}[POX] \text{ where } k_1[PAM/HA] \approx k_{obsd} \quad \text{Eq 2}$$

$$\ln[POX]_t = \ln[POX]_{t=0} - k_{obsd}t \quad \text{Eq 3}$$

$$t_{1/2} = \ln(2)/k_{obsd} \quad \text{Eq 4}$$

pH model of POX hydrolysis

The pH-rate (k_1) curves were simulated under an assumption that POX hydrolysis occurs via two parallel catalytic pathways—one through a neutral species, and the other through an anionic species (Figure 3). We applied the weighted linear combination of the two pathways, each dependent on the fraction (Fr) of either a neutral species (oxime/HA) or an anionic species (oximate/hydroxamate) (Eq 5–Eq 7). The fraction of core deprotonation for a test compound was calculated according to its core pK_a-pH approximation.[36] A curve fitting of k_1 versus pH was made through a linear combination of two fractional rate constants using $k_{1,\text{ oxime}}$ (≈ $k_{1,\text{ pH 7.4}}$) and $k_{1,\text{ oximate}}$ (≈ $k_{1,\text{ pH 10.5}}$) (Eq 7).

Rate = rate (Oximate) + rate (Oxime) Eq 5

$$\text{Rate} = -d[\text{POX}]/dt \approx k_{1,\text{oximate}}[\text{Oximate}][\text{POX}] + k_{1,\text{oxime}}[\text{Oxime}][\text{POX}] \quad \text{Eq 6}$$

$$\text{Rate} \approx (k_{1,\text{oximate}} \cdot \text{Fr}_{\text{oximate}} + k_{1,\text{oxime}} \cdot \text{Fr}_{\text{oxime}})[\text{Oxime} + \text{Oximate}]_{\text{total}}[\text{POX}] \text{ where } (\text{Fr}_{\text{oximate}} + \text{Fr}_{\text{oxime}}) = 1 \quad \text{Eq 7}$$

Skin decontamination *ex vivo*

Porcine skin was used as the test membrane for POX decontamination in a Franz cell device with a water jacket controlled at 37 ºC. The dehaired skin (1.5 mm thick; Stellen Medical, LLC) was clamped between the donor and receptor chambers. A solution of POX (0.4 mL, 50 μM) in PBS pH 10.5 containing 0.5% DMSO was added to the donor chamber. After 2 min exposure, a solution (0.4 mL) of Dekon 139 or a test compound (**7**, **17**, **23**, **30**), each formulated at 0.3 M in PBS pH 10.5, was added to the POX solution in the donor side. The PBS pH 10.5 vehicle alone was also tested as a control. After the decontaminant addition, analyte samples were taken from the solution in the donor side at specific time points (t = 0, 6, 15, 30, 60, and 120 min) and from the receptor side at t = 120 min. After 2 h of treatment, each skin sample was recovered, thoroughly rinsed with PBS, and weighed. Skin was cut into small pieces, and POX was extracted in 100% ethanol (1.0 mL) on a shaker at room temperature overnight. Samples were centrifuged at 2,000 rpm, and the supernatant was filtered through a nylon cell strainer to obtain clarified extract.

Sample solutions from the donor side were analysed by UPLC as detailed in the SI. The concentration of intact POX in each sample was determined from the area under curve (AUC) analysis of its peak relative to its calibration curve prepared from a series of standards with known POX concentrations (50 μM–0.1 μM). The POX half-life was calculated from the exponential decay of the AUC values over time.

Samples of skin extracts and the flow-through in the receptor chamber were analysed by LCMS mass spectrometry using an injection volume of 10 μL as described below. The concentration of POX was determined from the AUC value of the POX peak compared to its standard calibration curve. The total amount of POX (ng) was calculated, and used to calculate the rate of skin penetration (unit = POX ng/(skin tissue g × h)) measured in a skin sample (g) after 2 h exposure.

POX analysis by mass spectrometry

LCMS spectrometry spectrometry (Waters Acquity UPLC system equipped with a Waters TQ detector mass spectrometer) was employed for quantitative analysis of POX from samples collected in the skin decontamination experiment. The chromatographic system had an ODS column (Acquity UPLC BEH C18 1.7 μm; 2.1 × 100 mm, with an XBridge C18 2.5 μm guard column, Waters) at a column temperature of 40 °C with a flow rate of 0.45 mL/min. Column elution was performed using a gradient mode with two mobile phases: 95% A (0–0.25 min), 95–0% A (0.25–7.75 min), 0% A (7.75–8.5 min), 0–95% A (8.5–8.51 min) over a 10 min cycle. Mobile phase A = 0.1% formic acid in 98:2 water:methanol; Mobile phase B = 0.1% formic acid in methanol.

POX was detected using a method of multiple reaction monitoring (MRM) parameters (positive ionization mode; source temperature = 150 ^{o}C; desolvation temperature = 400 ^{o}C; cone voltage = 27 V; collision energy = 20 eV). POX was identified as the species at t_r = 6.0 min in the LC trace which produced a parent mass (m/z) of 276.036. A calibration curve for POX was generated in the range of 1.0 nM to 1000 nM: AUC = slope × [POX] (slope = 1640.6, R^2 = 0.996).

Acetylcholine esterase (AChE) assay

The enzymatic assay used AChE from *Electrophorous electricus* (Sigma-Aldrich) and thioacetylcholine as the substrate in PBS, pH 8.0 at 23 °C.[40, 50, 51] Reaction kinetics were measured spectrophotometrically at 412 nm using a 96-well microplate in a plate reader. For enzyme reactivation, AChE (0.1 U/mL) was completely inhibited to ≥95% by pre-incubation with POX (500 nM) for 60 min prior to treatment with 2-PAM or a test compound over a range of test concentrations (10^{-7}–10^{-3} M).

The efficiency of enzyme reactivation is reported as % activity as previously established:[52] AChE activity (%) = 100 × $[(k_{\text{oxime}} - k_{\text{POX-inactive}})/(k_{\text{active}} - k_{\text{POX-inactive}})]$ where each of the terms refers to a first-order rate constant k (dA/dt; min^{-1}) determined from a fully active enzyme (k_{active}), the POX-inactivated enzyme ($k_{\text{POX-inactive}}$), or the POX-inactivated enzyme after an oxime treatment (k_{oxime}). The activity of enzyme inhibition by an oxime compound alone is reported as % inhibition which was calculated as: Enzyme Inhibition (%) = 100 × ($k_{\text{oxime}}/k_{\text{active}}$).

Hazardous Materials

Caution: The following chemicals are hazardous and should be handled carefully: paraoxon-ethyl (POX), malaoxon, and omethoate.[1]

Statistical analysis

Analysis of statistical significance was performed by one-way ANOVA with GraphPad Prism 7 software. Differences with p values of <0.05 are reported as statistically significant.

Supporting information

Details of materials and analytical methods not detailed above, synthetic methods, copies of NMR and UV–Vis spectra, supplementary figures and tables.

Conflicts of interest

The authors declare no competing financial interest.

Acknowledgments

This work was supported by the US Defense Threats Reduction Agency–DOD (HDTRA1-17-C-00001).

Notes and references

1 J. Bajgar, in *Advances in Clinical Chemistry*, ed. S. M. Gregory, Elsevier, 2004, vol. Volume 38, pp. 151–216.
2 J. A. Vale, *Toxicology*, 2007, **240**, 141–142.
3 J. C. DeMar, E. D. Clarkson, R. H. Ratcliffe, A. J. Campbell, S. G. Thangavelu, C. A. Herdman, H. Leader, S. M. Schulz, E. Marek, M. A. Medynets, T. C. Ku, S. A. Evans, F. A. Khan, R. R. Owens, M. P. Nambiar and R. K. Gordon, *Chem.-Biol. Interact.*, 2010, **187**, 191–198.
4 R. K. Sit, Z. Radić, V. Gerardi, L. Zhang, E. Garcia, M. Katalinić, G. Amitai, Z. Kovarik, V. V. Fokin, K. B. Sharpless and P. Taylor, *J. Biol. Chem.*, 2011, **286**, 19422–19430.
5 C. A. Broomfield, O. Lockridge and C. B. Millard, *Chem.-Biol. Interact.*, 1999, **119–120**, 413–418.
6 O. Cohen, C. Kronman, L. Raveh, O. Mazor, A. Ordentlich and A. Shafferman, *Mol. Pharmacol.*, 2006, **70**, 1121–1131.
7 D. Jun, L. Musilová, M. Link, M. Loiodice, F. Nachon, D. Rochu, F. Renault and P. Masson, *Chem.-Biol. Interact.*, 2010, **187**, 380–383.
8 S. Bharathi, P. T. Wong, A. Desai, O. Lykhytska, V. Choe, H. Kim, T. P. Thomas, J. R. Baker and S. K. Choi, *J. Mater. Chem. B*, 2014, **2**, 1068–1078.
9 S. Tang, P. T. Wong, J. Cannon, K. Yang, S. Bowden, S. Bhattacharjee, J. J. O'Konek and S. K. Choi, *Chem.-Biol. Interact.*, 2019, **297**, 67–79.
10 M. Fentabil, M. Gebremedhin, J. G. Purdon, L. Cochrane and V. S. Goldman, *Toxicol. Lett.*, 2018, **293**, 241–248.
11 N. Singh, Y. Karpichev, R. Sharma, B. Gupta, A. K. Sahu, M. L. Satnami and K. K. Ghosh, *Org. Biomol. Chem.*, 2015, **13**, 2827–2848.
12 M. C. Franklin, M. J. Rudolph, C. Ginter, M. S. Cassidy and J. Cheung, *Proteins: Struct., Funct., Bioinf.*, 2016, **84**, 1246–1256.
13 B. t. Sanson, F. Nachon, J.-P. Colletier, M.-T. r. s. Froment, L. Toker, H. M. Greenblatt, J. L. Sussman, Y. Ashani, P. Masson, I. Silman and M. Weik, *J. Med. Chem.*, 2009, **52**, 7593–7603.
14 D. Jovanović, *Arch. Toxicol.*, 1989, **63**, 416–418.
15 J. Misik, R. Pavlikova, D. Josse, J. Cabal and K. Kuca, *Toxicol. Mech. Methods*, 2012, **22**, 520–525.
16 S. Bjarnason, J. Mikler, I. Hill, C. Tenn, M. Garrett, N. Caddy and T. Sawyer, *Hum. Exp. Toxicol.*, 2008, **27**, 253–261.
17 P. Li, S.-Y. Moon, M. A. Guelta, L. Lin, D. A. Gómez-Gualdrón, R. Q. Snurr, S. P. Harvey, J. T. Hupp and O. K. Farha, *ACS Nano*, 2016, **10**, 9174–9182.
18 G. Amitai, H. Murata, J. D. Andersen, R. R. Koepsel and A. J. Russell, *Biomaterials*, 2010, **31**, 4417–4425.
19 J. I. Morales, R. Figueroa, M. Rojas, D. Millán, R. A. Tapia and P. Pavez, *Org. Biomol. Chem.*, 2018, **16**, 7446–7453.
20 J. S. W. Tsang, A. A. Neverov and R. S. Brown, *Org. Biomol. Chem.*, 2004, **2**, 3457–3463.
21 P. Jacquet, D. Daudé, J. Bzdrenga, P. Masson, M. Elias and E. Chabrière, *Environ. Sci. Pollut. Res.*, 2016, **23**, 8200–8218.
22 E. H. Braue, K. H. Smith, B. F. Doxzon, H. L. Lumpkin and E. D. Clarkson, *Cutaneous Ocul. Toxicol.*, 2011, **30**, 15–28.
23 M. W. Fryer, P. W. Gage, I. R. Neering, A. F. Dulhunty and G. D. Lamh, *Pfluegers Arch.*, 1988, **411**, 76–79.
24 G. Becker, A. Kawan and L. Szinicz, *Arch. Toxicol.*, 1997, **71**, 714–718.
25 J. C. Lamb, G. M. Steinberg, S. Solomon and B. E. Hackley, *Biochemistry*, 1965, **4**, 2475–2484.
26 E. J. Behrman, M. J. Biallas, H. J. Brass, J. O. Edwards and M. Isaks, *J. Org. Chem.*, 1970, **35**, 3069–3075.
27 F. Terrier, P. Rodriguez-Dafonte, E. Le Guevel and G. Moutiers, *Org. Biomol. Chem.*, 2006, **4**, 4352–4363.
28 B. E. Hackley, R. Plapinger, M. Stolberg and T. Wagner-Jauregg, *J. Am. Chem. Soc.*, 1955, **77**, 3651–3653.
29 R. Swidler and G. M. Steinberg, *J. Am. Chem. Soc.*, 1956, **78**, 3594–3598.
30 S. B. Bharate, L. Guo, T. E. Reeves, D. M. Cerasoli and C. M. Thompson, *Bioorg. Med. Chem. Lett.*, 2009, **19**, 5101–5104.
31 E. J. Poziomek, B. E. Hackley and G. M. Steinberg, *J. Org. Chem.*, 1958, **23**, 714–717.
32 J. Hadgraft and W. John Pugh, *J. Invest. Dermatol. Symp. Proc.*, 1998, **3**, 131–135.
33 J. D. Bos and M. M. H. M. Meinardi, *Exp. Dermatol.*, 2000, **9**, 165–169.
34 J. Sangster, *Octanol-Water Partition Coefficients: Fundamentals and Physical Chemistry.*, John Wiley & Sons Ltd, Chichester, 1997.
35 C. A. Boulet and A. S. Hansen, *Phosphorus, Sulfur, and Silicon and the Related Elements*, 1991, **57**, 147–161.
36 H. N. Po and N. M. Senozan, *J. Chem. Educ.*, 2001, **78**, 1499.
37 F. Worek, G. Reiter, P. Eyer and L. Szinicz, *Arch. Toxicol.*, 2002, **76**, 523–529.
38 F. Worek, H. Thiermann, L. Szinicz and P. Eyer, *Biochem. Pharmacol. (Amsterdam, Neth.)*, 2004, **68**, 2237–2248.
39 J. A. Berberich, T. R. Stouch, S. Manepalli, E. X. Esposito and J. D. Madura, *Chem. Res. Toxicol.*, 2016, **29**, 1534–1540.
40 G. L. Ellman, K. D. Courtney, V. Andres jr and R. M. Featherstone, *Biochem. Pharmacol. (Amsterdam, Neth.)*, 1961, **7**, 88–95.
41 P. Demerseman, D. Kiffer, L. Debussche, C. Lion, R. Royer and H. Sentenac-Roumanou, *Eur. J. Med. Chem.*, 1988, **23**, 63–68.
42 K. B. Wallace and U. Herzberg, *Toxicol. Appl. Pharmacol.*, 1988, **92**, 307–314.
43 D. Jun, L. Musilova, K. Musilek and K. Kuca, *Int. J. Mol. Sci.*, 2011, **12**, 2077–2087.
44 G. A. Petroianu, K. Arafat, S. M. Nurulain, K. Kuča and J. Kassa, *J. Appl. Toxicol.*, 2007, **27**, 168–175.
45 T. Zorbaz, A. Braïki, N. Maraković, J. Renou, E. de la Mora, N. Maček Hrvat, M. Katalinić, I. Silman, J. L. Sussman, G. Mercey, C. Gomez, R. Mougeot, B. Pérez, R. Baati, F. Nachon, M. Weik, L. Jean, Z. Kovarik and P.-Y. Renard, *Chem. - Eur. J.*, 2018, **24**, 9675–9691.
46 S. K. Choi, P. Leroueil, M.-H. Li, A. Desai, H. Zong, A. F. L. Van Der Spek and J. R. Baker Jr, *Macromolecules*, 2011, **44**, 4026–4029.
47 S. K. Choi, T. P. Thomas, P. R. Leroueil, A. Kotlyar, A. F. L. Van Der Spek and J. R. Baker, *J. Phys. Chem. B*, 2012, **116**, 10387–10397.
48 J. Mukherjee, P. T. Wong, S. Tang, K. Gam, A. Coulter, J. R. Baker and S. K. Choi, *Mol. Pharmaceutics*, 2015, **12**, 4498–4508.
49 M. J. Vicent, H. Ringsdorf and R. Duncan, *Adv. Drug Delivery Rev.*, 2009, **61**, 1117–1120.
50 R. Cochran, J. Kalisiak, T. Küçükkılınç, Z. Radić, E. Garcia, L. Zhang, K.-Y. Ho, G. Amitai, Z. Kovarik, V. V. Fokin, K. B. Sharpless and P. Taylor, *J. Biol. Chem.*, 2011, **286**, 29718–29724.
51 M. C. de Koning, G. Horn, F. Worek and M. van Grol, *Eur. J. Med. Chem.*, 2018, **157**, 151–160.
52 G. E. Garcia, A. J. Campbell, J. Olson, D. Moorad-Doctor and V. I. Morthole, *Chem.-Biol. Interact.*, 2010, **187**, 199–206.